Calibrated photoacoustic spectrometry with an imaging system

Mitradeep Sarkar, Gilles Renault, Jérôme Gateau

Calibrated photoacoustic spectrometry with an imaging system

MITRADEEP SARKAR,[1] GILLES RENAULT,[2] JEROME GATEAU[3,*]

[1]Université de Paris, Inserm, PARCC, F-75015 Paris, France
[2] Université de Paris, Institut Cochin, INSERM, CNRS, F-75014 PARIS, France
[3] Sorbonne Université, CNRS, INSERM, Laboratoire d'Imagerie Biomédicale, LIB, F-75006, Paris, France
*Corresponding author: jerome.gateau@sorbonne universite.fr

Photoacoustic (PA) contrast agents are usually characterized with spectrophotometry or uncalibrated PA imaging systems, leading to partial assessment of their PA efficacy. To perform calibrated PA spectroscopy with a PA imaging system, we developed a method that both corrects for the spectral energy distribution of excitation light and performs a conversion from arbitrary to spectroscopic units, using a reference solution of cupric sulfate. The method was implemented on an imaging set-up based on a tunable laser and a 5MHz ultrasound array. We demonstrated robust calibrated spectroscopy on 15µL sample volumes of known chromophores and commonly used PA contrast agents, and for multiple samples simultaneously. The detection was linear with the absorption and the sensitivity below 0.08cm^{-1}.

Photoacoustic imaging (PAI) is an emerging multi-wave biomedical imaging modality able to reveal functional and molecular information at centimeter-depth and in sub-millimeter resolution [1]. PAI is based on the photoacoustic (PA) effect: optically absorbing structures within the tissue emit ultrasound waves when excited with a transient illumination. The ultrasound waves are generated by thermoelastic expansion and their amplitude is proportional to the absorption coefficient at the excitation wavelength. Therefore, successive acquisitions of images at different optical wavelengths allow spectral discrimination and quantification of the various absorbers in the imaged region [2].

To enhance this hybrid imaging modality beyond the information brought by endogenous absorbers like hemoglobin, absorbing exogenous contrast agents can be injected [3]. Recently, the material science community has shown a growing interest for the development of novel PA contrast agents [4,5], resulting in a strong need for their characterization in terms of effective PA spectra and their efficiency to generate ultrasounds. Spectrophotometery (SPP), based on the reflection or transmission of light by the sample, usually measures the optical attenuation: the sum of the absorption and the scattering, while the latter do not contribute to the PA signal generation. Moreover, SPP do not account for the photo-physic and thermo-elastic processes that occur between the optical absorption and the ultrasound generation.

Several PA spectrometers have already been developed. However, either they are calibrated but do not use a PAI system or they use PAI but are not calibrated. More precisely, Beard et al [6–8] developed a PA spectrometer able to measure the absolute absorption coefficient by a fit to the ultrasound signal. Additionally, photoacoustic specific coefficient such as the photothermal conversion efficiency E_{pt}, which represents the conversion efficiency of the absorbed energy to heat, and the Grüneisen coefficient Γ (relative to water), which describes the conversion of the heat energy to ultrasound waves could be determined. However, this PA spectrometer requires large sample volumes (mL) and a specific ultrasound detector with a very broadband and flat frequency response. Other PA spectrometers based on dedicated single-element detectors, but with less requirements on the ultrasound frequency response, showed measurement of the absorption coefficient thanks to a calibration with a reference solution [9,10]. For these PA spectrometers, small sample volumes (3µL [10] and 200µL [9]) are placed in optical transparent cells and SPP is performed on the same sample to retrieve the product E_{pt} Γ. Only one sample can be tested at a time and the sample size was poorly adapted to the frequency response of the detector. Commercial PAI systems [11,12] were also used to measure the PA spectral response of contrast agents. However, no calibration was performed leading to arbitrary units and sample sizes were at least 10 times too large for the center frequency of the detectors.

We have developed and we present herein a calibration method which uses a reference solution to transform a PAI system into a calibrated PA spectrometer. We implemented the method in a standard configuration for PAI [13]: a clinical linear ultrasound detector array with light delivered from the side (Fig. 1a). For PA characterization, small sample volumes (15µL) were injected in tubes whose diameter was chosen so that the ultrasound emission matches the frequency bandwidth of the detector. We demonstrate that our simple experimental setup enables robust calibrated spectroscopic measurement of several samples in parallel.

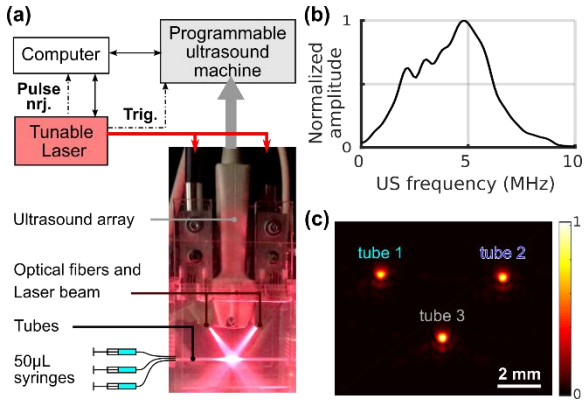

Fig. 1 Experimental setup (a) Annotated picture of the PAI system and schematic drawing of the experimental setup. (b) Frequency spectrum of the PA generated ultrasound signal. (c) Image of 3 tubes filled with the reference solution.

The experimental setup is presented in Fig. 1. A tunable (680-980 nm) optical parametric oscillator laser (SpitLight 600 OPO, Innolas) delivering < 8 ns pulses with a pulse repetition frequency of 20 Hz was used to generate the excitation light. Ultrasounds were detected with a 128-element clinical linear array (L7-4, 5MHz center frequency, ATL) driven by a programmable ultrasound machine used in receive-only mode (Vantage, Verasonics). A fiber bundle with two arms (CeramOptec GmbH) guided the light to the sample. In each arm, fibers were oriented toward the elevation focus of the array (Fig. 1a) and delivered light over the entire length of the array. The maximum fluence at the acoustic focus was 4.5 mJ.cm^{-2} at 750 nm. Each laser pulse triggered an ultrasound acquisition and a recording of the pulse energy using a non-calibrated pyrometer incorporated in the laser. Samples were injected in 50-cm long PTFE tubes (inner diameter: 0.2mm, wall thickness: 0.1mm, Bola) placed perpendicularly to the imaging plane and near the acoustic focus (25mm). PTFE was used for its weak optical absorption [14]. The illuminated length was ~ 1.5 cm. The inner volume of a tube was 15µL, and the tubes were filled using a 33-gauge needle and a 50µL gas tight syringe (Hamilton). The tubes were immersed in a water tank at room temperature to ensure acoustic coupling between the sample and the ultrasound detector. Given the inner diameter of the tubes, the ultrasound waves generated by sample are expected to be broadband with the maximum emission frequency around 4 MHz [15]. The ultrasound spectrum of measured PA signals indeed covers the bandwidth of the detector and has a peak at 5 MHz (Fig. 1c), which demonstrates the match between the detector and the sample container.

Once the solutions of contrast agents are in the tubes, the spectrum measurement consists of acquiring the ultrasound signals and the pyrometer values for 30 successive sweeps of the optical wavelengths (λ) between 680nm to 970 nm by steps of 10 nm. This acquisition sequence avoids consecutive excitations at a given wavelength that could induce photodegradation, and enables to detect potential spectral changes during the acquisition as the whole spectral range is covered 30 times. For all samples tested in this paper, the spectra were found stable. Therefore, iterations at a given wavelength were averaged to increase the signal-to-noise ratio. As for every PA spectrometer, before averaging, ultrasound signals were corrected for the pulse-to-pulse energy fluctuations of the laser, by dividing them by the corresponding pyrometer value.

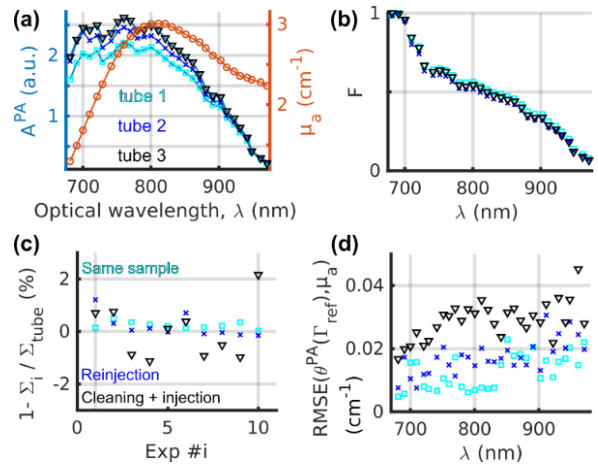

Fig. 2 Calibration method of the PA spectrometer with the reference solution of $CuSO_4$, $5H_2O$. (a) PA amplitudes derived from the image A^{PA} for three different tubes (left) and the decadic absorption coefficient measured with the spectrophotometer μ_a (right). (b) Normalized factor $F(\lambda)$ for the correction of subsequent spectra for each tube. The factor Σ_{tube} was determined to be equal to $\Sigma_{tube\ 1}$ = 1.07cm, $\Sigma_{tube\ 2}$ =1.27cm and $\Sigma_{tube\ 3}$=1.29cm, respectively. (c) Relative deviation of Σ for 10 measurements. (d) Root-mean-square error (RSME) of the PA spectrum with respect to μ_a.

Post-processing of the averaged signals to obtain the calibrated PA spectrum of a sample requires the measurement of two additional solutions that are successively injected in the same tube: 1) water, as a reference for the background absorption, 2) a solution with known absorption and photoacoustic properties, as a reference for calibration. We chose an aqueous solution of cupric sulfate pentahydrate ($CuSO_4$,$5H_2O$, Sigma-Aldrich), as this chromophore has been previously fully characterized photoacoustically [8]. Between two injections, the tube was flushed with air and water to clean it and again with air to avoid dilution of the next sample. The averaged signals for water were coherently subtracted from the averaged signals of the sample, and the Hilbert transform was computed to obtain quadrature signals. The signals and quadrature signals were beamformed using a simple delay-and-sum image reconstruction algorithm. Then, an envelope-detected image was computed from the root-mean square of the two images for each pixel. Each tube appears as a Gaussian spot. (Fig. 1c), and its amplitude (A^{PA}) was determined using a 2D Gaussian fit. . Because the illumination and the ultrasound detector have a finite size and are directional, A^{PA} significantly depends on the spatial location of the tube (Fig. 2a). A^{PA} can be decomposed as:

$$A^{PA}(\lambda) = \alpha_{tube}(\lambda).\xi_{sample}(\lambda) \qquad (1)$$

where α_{tube} depends on the location of the tube in the experimental setup, and ξ_{sample} depends on the PA properties of the sample. As thermal and stress confinements are verified for the dimension of the tube [16], theoretically we have:

$$\xi_{sample}(\lambda) = E_{pt}.\Gamma_{sample}/\Gamma_{water}.\mu_a(\lambda) \qquad (2)$$

where E_{pt} and Γ_{sample} are, respectively, the photothermal conversion efficiency and the Grüneisen coefficient of the sample solution, μ_a its decadic absorption coefficient and Γ_{water} is the Grüneisen coefficient of water. On the other hand, α_{tube} comprises of the local light fluence and the conversion factor between the

arbitrary units of A^{PA} and the spectroscopic units of ξ_{sample}. We express α_{tube} as the product of Σ, a constant factor, and F(λ), the normalized (to its maximum) product of the spectral energy distribution of the laser and the pyrometer spectral sensitivity.

The calibration process consists in determining $\alpha_{tube}(\lambda)$ with the reference solution: a aqueous solution of $CuSO_4$, $5H_2O$ at a concentration of 0.25M, with a calculated ratio $\Gamma_{ref}/\Gamma_{water} = 1.18$ and $E_{pt}=1$ [8]. This reference solution is photostable, absorbs and do not scatter over the investigated spectral range. Its absorption coefficient μ_a (Fig. 2a) was measured with SPP (Perkin Elmer lambda 950 UV/VIS/NIR). F(λ) was determined from the normalized ratio of A^{PA} and μ_a. Then, $A^{PA}.\Gamma_{water}/(F.\Gamma_{ref})$ was fitted to μ_a to find Σ.

The calibration was performed simultaneously for three tubes located approximately 5 mm apart (Fig. 1c). Although it has similar values, F(λ) slightly differs for the three tubes (Fig. 2b). Subsequently to the calibration, we validated its robustness by performing a series of 10 measurements in the tubes. In tube 1, the reference solution was left to assess the intrinsic measurement fluctuations. For Tube 2, 50µl of the reference solution was injected again (without flushing with water and air) to measure the variations due to reinjection. Tube 3 was cleaned with water and air, and the reference solution was injected between successive acquisitions. For all the series and for each tube, the F(λ) determined during the calibration phase was applied. A correction factor Σ_i was estimated for each experiment and compared to Σ_{tube} determined in the initial calibration (Fig. 2c). Maximal relative deviations of 0.5% for tube 1, 1.2 % for tube 2 and 2.2 % for tube 3 were found. The small deviation values validate the global stability of the acquisition process. The main source of fluctuations was found to come from the injection with cleaning.

To quantify the variations at each optical wavelength, we compare our PA estimate of the decadic absorption coefficient $\theta^{PA}(\Gamma_{sample},\lambda) = A^{PA}(\lambda).\Gamma_{water}/(E_{pt}.\Gamma_{sample}.\alpha_{tube}(\lambda))$ with respect to the SPP measurement of μ_a. We compute the root-mean-square error, named RSME(θ^{PA}, μ_a) and defined as:

$$RSME(\theta^{PA},\mu_a) = \sqrt{\frac{1}{n}\sum_{i=1}^{n}(\theta_i^{PA}-\mu_a)^2} \qquad (3)$$

where n =10 is the number of acquisitions, and θ_i^{PA} is obtained with α_{tube} estimated in the initial calibration and the parameters of the reference solution. Fig. 2d shows a RSME(θ^{PA}, μ_a) below 0.05 cm^{-1}. This validates the stability of the measurements over the whole spectral range. The largest error values were for tube 3 because of the global amplitude fluctuations (Fig. 2c).

The calibration obtained with the reference solution was validated with two other sample solutions for which the Grüneisen coefficient could be calculated [8] and the absorption spectrum measured by SPP: an aqueous solution of nickel sulfate ($NiSO_4$,$6H_2O$, Sigma-Aldrich) at 1.66 M ($\Gamma_{NiSO4}/\Gamma_{water}$ =1.54), and a solution of $CuSO_4.5H_2O$ at 0.125M and $NiSO_4.6H_2O$ at 0.85 M (named Mix, $\Gamma_{Mix}/\Gamma_{water}$=1.36). For each sample, the measurements were repeated 10 times (two tubes with 5 injections each with a cleaning) after an initial calibration. Fig. 3a shows that the spectral shapes of θ^{PA} and μ_a match for the two samples. The experimental Grüneisen coefficients of the two solutions were estimated by fitting A^{PA}/α_{tube} with μ_a, considering $E_{pt}=1$. We found $\Gamma_{NiSO4}/\Gamma_{water}$=1.87±0.02 (mean±std) and $\Gamma_{Mix}/\Gamma_{water}$=1.64±0.04 (Fig. 3b). As expected, Γ_{NiSO4} was higher than Γ_{Mix}. However, the ratios Γ/Γ_{water} were consistently 21% higher than the calculated values. As $NiSO_4$ dominates the calculation of Γ/Γ_{water}, the variation could be attributed to the sample batch.

The RSME(θ^{PA}(<Γ>),μ_a), where <Γ> is the experimental mean Grüneisen coefficient, is of the same order as for the reference solution (Fig. 3c), with a dominance of the global amplitude fluctuation of θ^{PA} on the error.

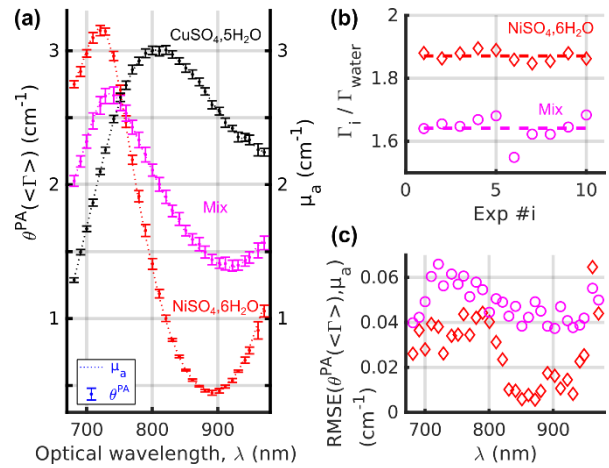

Fig. 3 Validation of the calibration method to obtain the spectral shape and the Grüneisen coefficient of solutions. (a) θ^{PA} (<Γ>) with <Γ> the mean Grüneisen coefficient of each solution (<Γ_{CuSO4}> = Γ_{ref}) (left) and decadic absorption coefficient μ_a (right). (b) Estimated Grüneisen value over 10 successive measurements. (c) Root-mean-square error (RSME) between θ^{PA} and μ_a for each solution. The same colors as for (b) are used. The errors bars in (a) represent the RSME shown in (c).

The linearity and the sensitivity of the spectrometer were assessed by measuring solutions of $CuSO_4$, $5H_2O$ at different concentrations (c_{CuSO4}) from 7 mM to 0.25M. The Grüneisen coefficient Γ_c was computed for each c_{CuSO4} [8]. The PA spectrum could be measured down to 0.08 cm^{-1} (Fig. 4a), and it matches the SPP spectrum of the reference solution scaled by the dilution factor. Water samples (c_{CuSO4}=0) were measured 10 times and the standard deviation of $\theta^{PA}(\Gamma_{water})$ had similar values as for the RSME (Fig. 2d). Fig. 4b demonstrates the linearity of $\theta^{PA}(\Gamma_c)$ over more than one order of magnitude of concentrations for three optical wavelengths.

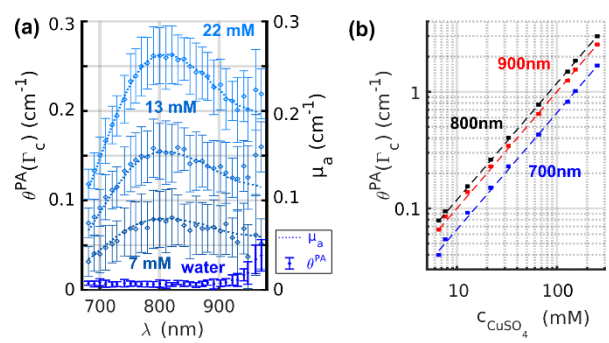

Fig. 4. Linearity and sensitivity of the PA spectrometer. (a) $\theta^{PA}(\Gamma_c)$ where Γ_c is the calculated Grüneisen coefficient at each concentration of $CuSO_4$(left). μ_a of the reference solution scaled to account for the dilution (right). The error bars correspond to the RSME of Fig. 2d,

except for the water where the error bar is the standard deviation over 10 acquisitions. (b) $\theta^{PA}(\Gamma_c)$ as a function of sample concentration at three different optical wavelengths in a log-log scale plot. The dashed lines are linear fits, therefore the slope in log-log scale is equal to 1 for all the wavelengths.

Finally, we applied our method to measure the PA spectrum of two commonly used contrast agents in *in vivo* PAI [3]: gold nanoparticles and a near-infrared dye. These contrast agents respectively have plasmonic and fluorescent properties. Therefore, they have different optical absorption mechanisms and PA characteristics. A dispersion of citrate capped gold nanorods (GNR) in water (10±2 nm diameter, 42±8 nm length, Sigma-Aldrich) with a nominal maximum extinction at 808 nm was measured with our PA spectrometer assuming E_{pt}=1 and Γ/Γ_{water} =1. The attenuation coefficient μ^{SPP} was measured in the range 680-900 nm by SPP (V650 Jasco). The spectral shapes match (Fig. 5a). However, θ^{PA} was found smaller than μ^{SPP} by a factor 0.77. This factor could be explained by the combination of two phenomena. First, the solution of GNR was scattering [17] and SPP did not separate absorption from scattering in the attenuation measurement. Second, the GNR is the heat source while water is the PA signal-generating medium. Interfacial thermal resistance to the heat transfer at the gold-water interface could lower the effective photothermal conversion efficiency [18].

A clinically approved near-infrared dye, indocyanine green (ICG Sigma-Aldrich) was diluted in Dulbecco's phosphate buffered saline (concentrated x1 Gibco) at three different concentrations (9µM, 24µM and 47µM) and PA measurements were done within one hour of preparation. IGC is unstable once prepared and we could not perform SPP measurements of the corresponding solutions. However, as expected from the literature [19], the PA emission peak was found around 800 nm with a shoulder around 740 nm (Fig. 5b). Assuming a photothermal conversion efficiency E_{pt} =1, we calculated a PA molar absorption coefficient of 4.6 10^4 cm^{-1} M^{-1} from θ^{PA}. This value is low compare to reported molar extinction coefficient (~10^5 $cm^{-1}.M^{-1}$ [19]), but compatible. Indeed, the absorption of ICG is strongly dependent on the solvent [19]. Moreover, as ICG is a fluorescent molecule, its photothermal conversion efficiency is below 1. Recently, Fuenzalida Werner et al [9] reported that θ^{PA} (with E_{pt} =1) was smaller than μ_a by a factor 0.87 at 795 nm in a different buffered saline.

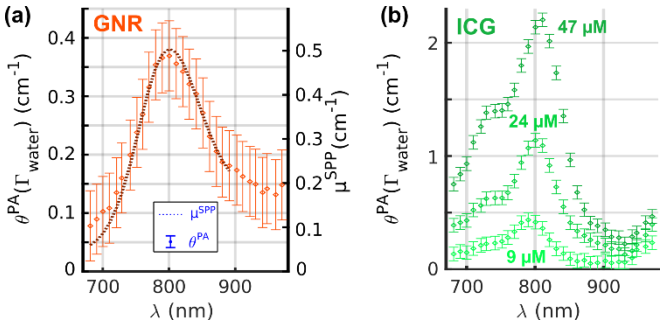

Fig. 5 Spectra of conventional contrast agents in *in vivo* PAI imaging. (a) Gold nanorods (GNR) with $\theta^{PA}(\Gamma_{water})$ (left) and the decadic attenuation coefficient measured with the spectrophotometer μ^{SP} (right). (b) $\theta^{PA}(\Gamma_{water})$ of indocyanine green (ICG) at 3 different concentrations. The error bars are +/- 0.06 cm^{-1} .

In this letter, we presented and validated a method to perform calibrated spectrometry with a commonly used PAI set-up. The method requires tubes that remain fixed during successive injections of different solutions: water as a background reference, a solution of $CuSO_4$, 5H2O as a calibration reference, and the sample of interest. The method can be adapted to various PAI systems, as long as they provide access to PA generated ultrasound signals and that the relative pulse-to pulse energy fluctuations of the excitation light at each wavelength can be recorded. We applied here the method to a PAI system based on a clinical ultrasound array and carefully adapted the sample size to the center frequency of the detector. Measurements were performed with sample volumes as low as 15 µL which enables PA measurements of new contrast agents at early stage of the development. We believe that our method can benefit to the growing need of characterization of PA contrast agents.

Funding. This work was supported by the MITI CNRS (Defi Imag'IN), Gefluc Paris- Ile de France, France Life Imaging (ANR-11-INBS-0006) and the FOLSMART project (H2020 N°68335). M. Sarkar acknowledges support from the Paris Region (Ile-de-France) under the Blaise Pascal International Chairs of Excellence. Imaging was performed at the Life Imaging Facility of Paris Descartes University (Plateforme Imageries du Vivant – PIV).

Acknowledgment. We thank F. Gazeau at MSC for fruitful discussions and her help in the fabrication of the sample holder. We thank J-S Lauret at the LAC for the NIR spectrophotometer.

References

1. P. Beard, "Biomedical photoacoustic imaging.," Interface Focus **1**, 602–31 (2011).
2. A. Taruttis and V. Ntziachristos, "Advances in real-time multispectral optoacoustic imaging and its applications," Nat Phot. **9**, 219–227 (2015).
3. J. Weber, P. C. Beard, and S. E. Bohndiek, "Contrast agents for molecular photoacoustic imaging.," Nat. Methods **13**, 639–50 (2016).
4. Y. Liu, P. Bhattarai, Z. Dai, and X. Chen, "Photothermal therapy and photoacoustic imaging *via* nanotheranostics in fighting cancer," Chem. Soc. Rev. (2018).
5. R. E. Borg and J. Rochford, "Molecular Photoacoustic Contrast Agents: Design Principles & Applications," Photochem. Photobiol. **94**, 1175–1209 (2018).
6. J. Laufer, E. Zhang, and P. Beard, "Evaluation of absorbing chromophores used in tissue phantoms for quantitative photoacoustic spectroscopy and imaging," IEEE J. Sel. Top. Quantum Electron. **16**, 600–607 (2010).
7. T. Stahl, T. Allen, and P. Beard, "Characterization of the thermalisation efficiency and photostability of photoacoustic contrast agents," Photons Plus Ultrasound Imaging Sens. 2014 **8943**, 89435H (2014).
8. M. Fonseca, B. Cox, M. Fonseca, L. An, P. Beard, B. Cox, M. Fonseca, L. An, P. Beard, and B. Cox, "Sulfates as chromophores for multiwavelength photoacoustic imaging phantoms," J. Biomed. Opt. **22**, 1 (2017).
9. J. P. Fuenzalida Werner, Y. Huang, K. Mishra, A. Chmyrov, V. Ntziachristos, and A. C. Stiel, "Challenging a preconception: Optoacoustic spectrum differs from the absorption spectrum of proteins and dyes for molecular imaging," BioRxiv (2020).
10. I. Pelivanov, E. Petrova, S. J. Yoon, Z. Qian, K. Guye, and M. O'Donnell, "Molecular fingerprinting of nanoparticles in complex media with non-contact photoacoustics: beyond the light scattering limit," Sci. Rep. **8**, 1–13 (2018).

11. P. Armanetti, A. Flori, C. Avigo, L. Conti, B. Valtancoli, D. Petroni, S. Doumett, L. Cappiello, C. Ravagli, G. Baldi, A. Bencini, and L. Menichetti, "Spectroscopic and photoacoustic characterization of encapsulated iron oxide super-paramagnetic nanoparticles as a new multiplatform contrast agent," Spectrochim. Acta - Part A Mol. Biomol. Spectrosc. **199**, 248–253 (2018).
12. C. J. H. Ho, G. Balasundaram, W. Driessen, R. McLaren, C. L. Wong, U. S. Dinish, A. B. E. Attia, V. Ntziachristos, and M. Olivo, "Multifunctional photosensitizer-based contrast agents for photoacoustic imaging," Sci. Rep. **4**, 1–6 (2014).
13. M. W. Schellenberg and H. K. Hunt, "Hand-held optoacoustic imaging: A review," Photoacoustics **11**, 14–27 (2018).
14. S. J. Arconada-Alvarez, J. E. Lemaster, J. Wang, and J. V. Jokerst, "The development and characterization of a novel yet simple 3D printed tool to facilitate phantom imaging of photoacoustic contrast agents," Photoacoustics **5**, 17–24 (2017).
15. M. I. Khan, T. Sun, and G. J. Diebold, "Photoacoustic waves generated by absorption of laser radiation in optically thin cylinders," J. Acoust. Soc. Am. **94**, 931–940 (1993).
16. M. Xu and L. V. Wang, "Photoacoustic imaging in biomedicine," Rev. Sci. Instrum. **77**, 1–22 (2006).
17. P. K. Jain, K. S. Lee, I. H. El-Sayed, and M. a. El-Sayed, "Calculated absorption and scattering properties of gold nanoparticles of different size, shape, and composition: Applications in biological imaging and biomedicine," J. Phys. Chem. B **110**, 7238–7248 (2006).
18. Y. S. Chen, W. Frey, S. Kim, P. Kruizinga, K. Homan, and S. Emelianov, "Silica-coated gold nanorods as photoacoustic signal nanoamplifiers," Nano Lett. **11**, 348–354 (2011).
19. M. L. Landsman, G. Kwant, G. A. Mook, and W. G. Zijlstra, "Light-absorbing properties, stability, and spectral stabilization of indocyanine green," J. Appl. Physiol. **40**, 575–583 (1976).